

# Electron-magnon scattering in an anisotropic half-metallic ferromagnetic Weyl semimetal $\text{Co}_3\text{Sn}_2\text{S}_2$

Shivam Rathod , Megha Malasi , Archana Lakhani , and Devendra Kumar \*

*UGC-DAE Consortium for Scientific Research, University Campus, Khandwa Road, Indore 452001, India*



(Received 22 April 2022; accepted 25 July 2022; published 26 August 2022)

$\text{Co}_3\text{Sn}_2\text{S}_2$  is a magnetic Weyl semimetal, anisotropic ferromagnet, and half-metal in a single material. These qualities modify the spin dynamics and behavior of electron-magnon scattering. We have investigated this unconventional ferromagnet for modified electron-magnon scattering behavior using temperature and magnetic field dependent resistivity.  $\text{Co}_3\text{Sn}_2\text{S}_2$  exhibits exponential suppression of spin-flip electron-magnon scattering below a characteristic crossover temperature which separates the regime of anomalous magnon scattering from one-magnon scattering. Interestingly, the Weyl fermion mediated spin dynamics with large magnetocrystalline anisotropy can also cause exponential suppression of electron-magnon scattering giving similar behavior in resistivity. The gap characterizing the suppression of electron-magnon scattering is 2.46(4) meV and increases linearly with magnetic field. The suppression of electron-magnon scattering could occur from half-metallic or anisotropic character but the presence of anomalous-magnon scattering at low temperatures evinces the half-metallic nature. A large anisotropy gap in magnon dispersion of half-metal can help prevent the deviation from 100% spin polarization at low temperatures.

DOI: [10.1103/PhysRevMaterials.6.084202](https://doi.org/10.1103/PhysRevMaterials.6.084202)

## I. INTRODUCTION

$\text{Co}_3\text{Sn}_2\text{S}_2$  is a kagome lattice half-metallic ferromagnet with Curie temperature ( $T_C$ ) around 177 K [1]. It exhibits a magnetic Weyl semimetallic state with novel physical properties like chiral magnetic effect from Weyl fermions [2], topological Fermi arc surface states [3–5], and large intrinsic anomalous Hall effect due to large Berry curvature of Weyl nodes [2,6]. Thus,  $\text{Co}_3\text{Sn}_2\text{S}_2$  provides a unique platform to study the physics connecting unconventional magnetism, band topology, and spintronics [7,8].

In half-metals, band structure at the Fermi level is gapless for one type of spin while gapped for another type of spin; therefore conduction electrons are spin-polarized. The electronic band structure calculations suggest spin-1/2 type I-A half-metallic ground state in  $\text{Co}_3\text{Sn}_2\text{S}_2$  [9,10] with magnetic moment  $1 \mu_B$  per f.u. [11]. Low-temperature angle-resolved photoemission studies and spin-resolved scanning tunneling spectroscopy support the presence of half-metallicity in  $\text{Co}_3\text{Sn}_2\text{S}_2$  [11–13]. On the other hand, the spin-polarized Andreev reflection spectroscopy in  $\text{Co}_3\text{Sn}_2\text{S}_2$  suggests that spin polarization is only 50% due to spin depolarization effects occurring at the Fermi level when spin-orbit coupling is included [8,14].

Half-metals are theoretically identified by calculation of band structure and integer spin moments [15]. Photoemission, scanning tunneling spectroscopy, and Andreev reflection experiments are surface sensitive and are susceptible to sample surface degradation, surface stoichiometry, and modification in electronic structures at the surface [14]. The identification of half-metal and degree of spin polarization with experiments is a challenging task [16,17]. Temperature-dependent

resistivity and magnetoresistance are bulk measurements and can in principle sensitively probe the half-metallicity from modified electron-magnon scattering behavior. There are several theories [17–23] for electron-magnon scattering in half-metals which are extensively utilized for identification of half-metallicity, for example in  $\text{CrO}_2$  [16,17,24–28], doped Heusler alloys [23,29–33], and perovskite manganites [18,34,35].

In half-metallic ferromagnets, because of unavailability of the minority spin band at the Fermi level, spin-flip scatterings are illegal [22,27,36]. The electron-magnon scattering in half-metallic systems is explained by the double-magnon scattering [22] mechanism for rigid electronic band structure. For the non-rigid-band approximation, the formation of shadowed minority bands at the Fermi level allows anomalous magnon scatterings [18]. Resistivity in half-metals due to suppression of electron-magnon scattering can be phenomenologically described by thermally activated behavior  $T^2 \exp(-\Delta/T)$ , where  $\Delta_{k_B}$  is the gap between Fermi energy and the nearest minority spin band edge [16,17,23–28].

$\text{Co}_3\text{Sn}_2\text{S}_2$  is an anisotropic ferromagnet with easy  $c$  axis [2]. In anisotropic ferromagnets, the gap in magnon spectrum ( $\delta$ ) suppresses the electron-magnon scattering [37] at low temperatures which modifies the electron-magnon resistivity as  $\rho_M \propto T^2 \exp(-\delta/k_B T)$  [38–40]. This is widely utilized to scale magnon resistivity of anisotropic ferromagnets [37–44] and antiferromagnets [45,46]. The neutron scattering experiments on  $\text{Co}_3\text{Sn}_2\text{S}_2$  show a gap of 2.3 meV in the magnon spectrum at 4 K. A gap in the spectrum arises due to spin anisotropy energy from spin-orbit coupling which is estimated as 0.6 meV for  $\text{Co}_3\text{Sn}_2\text{S}_2$ . The observation of a relatively large gap in the experiment signifies the contribution from Weyl fermions in low-energy spin-wave excitations [47] and similar behavior has been observed in other metallic ferromagnets with the possibility of Weyl nodes [48,49]. The

\*deveniit@gmail.com

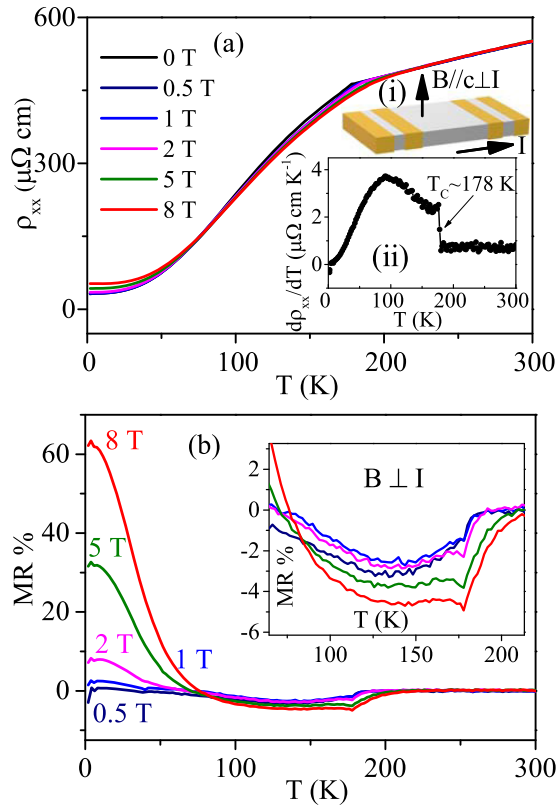


FIG. 1. (a) Resistivity versus temperature at different magnetic fields. The inset (i) displays the schematic of contacts for resistivity measurements and the inset (ii) shows the temperature derivative of resistivity. The magnetic field ( $B$ ) is parallel to the  $c$  axis and the current ( $I$ ) is in the plane perpendicular to the magnetic field and  $c$  axis. (b) Temperature dependence of magnetoresistance (MR) at different magnetic fields. The inset shows the expanded view of negative MR region.

half-metallicity of  $\text{Co}_3\text{Sn}_2\text{S}_2$  is still a dilemma while electron scattering mechanisms remain completely unexplored. Therefore, we investigate the electron-magnon scattering behaviors that can emerge in a half-metal or an anisotropic ferromagnetic Weyl semimetal.

## II. EXPERIMENTAL DETAILS

The high-quality  $\text{Co}_3\text{Sn}_2\text{S}_2$  single crystal used in this study is grown by the self-flux method [50,51]. The crystal is well characterized by x-ray diffraction, high-resolution x-ray diffraction, and energy-dispersive x-ray spectroscopy for phase purity and quality which is reported elsewhere [50,51]. The electrical resistivity measurements were performed by the standard four-probe ac technique using the ACT option of 9 T PPMS system. Four linear Ohmic contacts are made on the crystal with fine copper wires using indium.

## III. RESULTS AND DISCUSSION

Figure 1(a) shows the temperature dependence of resistivity ( $\rho_{xx}$ ) in the range of 2–300 K and magnetic field of 0–8 T applied parallel to the crystallographic  $c$  axis  $H$  [003]. The current is in the  $ab$  plane perpendicular to the field

direction. The temperature dependence of resistivity suggests the metallic behavior and the low residual resistivity  $\rho_{xx}(2\text{ K}) \approx 32.5\ \mu\Omega\text{ cm}$  and the high residual resistivity ratio  $\approx 17$  show the good crystal quality [51]. The resistivity exhibits a kink around paramagnetic to ferromagnetic transition temperature  $T_C \sim 178\text{ K}$  which further manifests as a jump in temperature derivative of resistance ( $d\rho_{xx}/dT$ ) shown in inset (ii) of Fig. 1(a). The temperature dependence of magnetoresistance  $\text{MR} = \{[\rho_{xx}(B) - \rho_{xx}(0)]/\rho_{xx}(0)\} \times 100$ , where  $\rho_{xx}(B)$  is in-field and  $\rho_{xx}(0)$  is zero-field resistivity, is shown in Fig. 1(b). On lowering the temperature below  $T_C$ , the magnetoresistance becomes negative and crosses over to positive values below 75 K. The negative MR persists above the technical saturation field [2] of  $\approx 0.05\text{ T}$  suggesting it cannot be ascribed to suppression of domain wall scattering. The inset of Fig. 1(b) shows that negative MR enhances on increasing the magnetic field and weakens on lowering the temperature below  $T_C$  suggesting the MR could be originating from spin-flip electron-magnon scattering. This is because the magnon population and thus the spin-flip electron-magnon scattering decreases on increasing the magnetic field and lowering the temperature. The low-temperature MR remains negative in normal band ferromagnets, but in half-metallic ferromagnets due to absence of minority bands, spin-flip scattering is exponentially suppressed for  $T < \Delta$  and the MR crosses over from negative to positive on decreasing the temperature [23]. The low-temperature positive MR is dominated by defects and Lorentz force in field.

Resistivity of a ferromagnet is due to scattering of conduction electrons from defects/impurities ( $\rho_o$ ), phonons ( $\rho_P$ ), and magnons ( $\rho_M$ ). According to Matthiessen's rule, the total resistivity is the sum of all contributing scattering mechanisms

$$\rho_{xx}(T, B) = \rho_o + \rho_P(T) + \rho_M(T, B), \quad (1)$$

where  $\rho_o$  is temperature independent and  $\rho_P$  is described by the Bloch-Grüneisen formula for contribution from acoustic phonons [52].  $\rho_P \propto T$  for  $T \gg \theta_D$  while  $\rho_P \propto T^5$  for  $T \ll \theta_D$ , where  $\theta_D$  is the Debye temperature.  $\rho_M \propto T^2$  for spin-flip electron-magnon scattering in isotropic ferromagnets which gets exponentially suppressed in half-metals and anisotropic ferromagnets. The  $\rho_o$  and  $\rho_P$  are nearly independent of external magnetic field while  $\rho_M$  decreases with field.

Equation (1) for conventional ferromagnets at  $T \ll \theta_D$  and  $T_C$  can be written as  $\rho_{xx} = \rho_o + a_2T^2 + a_5T^5$ , where  $a_2T^2$  is the electron-magnon scattering term and  $a_5T^5$  is from electron-phonon scattering. The low-temperature resistivity is scaled using the above equation and the fitting is shown in Fig. 2(a). The fit is not good which is evident from large difference in fitted and experimental data. Therefore  $\text{Co}_3\text{Sn}_2\text{S}_2$  cannot be treated like a normal isotropic ferromagnet and demands the search of other unconventional scattering mechanisms. The Debye temperature [53] of  $\text{Co}_3\text{Sn}_2\text{S}_2$  is around 369 K and the contributions from electron-phonon scattering are comparatively low ( $a_5 = 1.48 \times 10^{-8}$ ). Therefore, the temperature and field dependence of resistivity are mainly governed by  $\rho_M$ , i.e.,  $\rho_{xx}(T, B) \approx \rho_o + \rho_M$ .

The  $T^2$  dependence of  $\rho_M$  is for spin-flip or one-magnon scattering which occurs in conventional isotropic ferromagnets. In an itinerant ferromagnet, the magnetic electrons are conduction band electrons which travel through the crystal

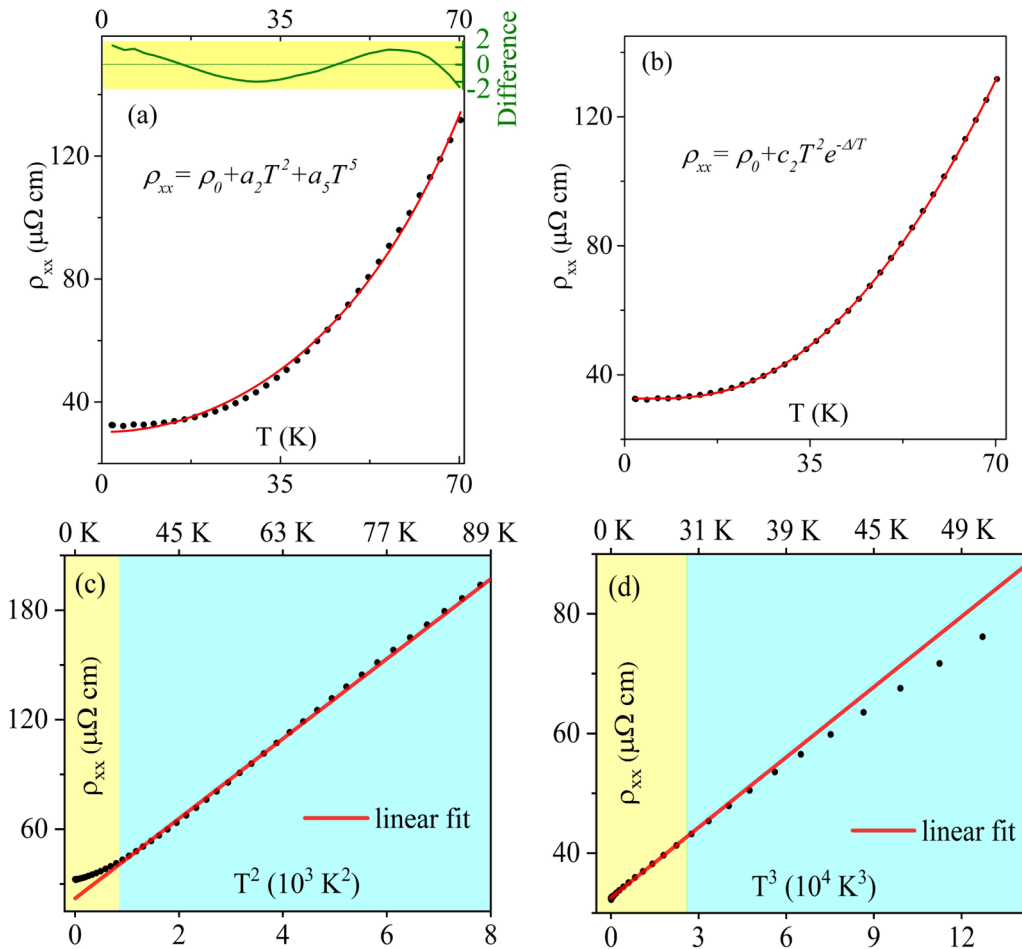


FIG. 2. (a) The temperature dependence of resistivity below 70 K. The red solid line shows the least-squares fitting of Eq. (1) for a conventional ferromagnet. The top inset shows the difference of experimental and fitted curve. (b) The temperature variation of resistivity along with least-squares fitting of  $\rho_{xx} = \rho_0 + c_2 T^2 \exp(-\Delta/T)$  (solid line). (c) The plot of  $\rho_{xx}$  vs  $T^2$  with linear fit (red line) showing the  $T^2$  behavior of resistivity at  $T > 28.5$  K and deviation below this temperature. (d)  $\rho_{xx}$  vs  $T^3$  with linear fit showing  $T^3$  behavior at low temperatures and deviation at higher temperatures. The light yellow and cyan color regions have boundary at  $\Delta = 28.5$  K.

but can also be considered partially localized to atomic sites [54,55]. The interaction of spin moments of conduction electrons and ions is the base of electron-magnon scattering [56]. At  $T = 0$  K, the spins associated with ions of a ferromagnetic metal are all parallel, while at finite temperatures, spin-waves or magnons are excited as displayed in Fig. 3(a). Each magnetic electron has its own set of bands as shown in Fig. 3(b) for ferromagnetic metal. The spin-up (or spin-down) electron by absorption or emission of only one quanta of spin wave does a spin-flip or one-magnon scattering (1MS) [22]. A spin-up electron with momentum  $k$  absorbs a magnon of momentum  $q$  and creates a spin-down electron of momentum  $q + k$  as shown in Fig. 3(c). The spin-flip scattering requires a minority spin band at the Fermi level ( $E_F$ ).

A schematic band diagram of a half-metallic ferromagnet is shown in Fig. 3(d), where the spin-up band is gapless while the spin-down bands are gapped at  $E_F$ . In such case, the  $T^2$  dependence of the electron-magnon spin-flip scattering is suppressed exponentially and is given by the phenomenological expression [17,22,23]

$$\rho_M = c_2 T^2 \exp(-\Delta/T), \quad (2)$$

where  $\Delta k_B$  is the gap between  $E_F$  and nearest minority spin band edge and  $c_2$  is related to strength of electron-magnon scattering. Figure 2(b) shows that the temperature dependence of resistivity can be well fitted with  $\rho_{xx} = \rho_0 + c_2 T^2 \exp(-\Delta/T)$  and the fitting gives  $\Delta = 28.5(5)$  K which corresponds to energy gap ( $\Delta k_B$ ) of 2.46(4) meV. The exponential suppression of  $T^2$  scattering suggests the half-metallicity in  $\text{Co}_3\text{Sn}_2\text{S}_2$ . According to band structure calculations [2], spin minority bands in  $\text{Co}_3\text{Sn}_2\text{S}_2$  are gapped  $\approx 100$  meV above  $E_F$ . The obtained gap = 2.46(4) meV is much smaller in comparison to the theoretically expected value of spin-flip gap 100 meV and similar variation in the experimental and theoretical values of gap has been observed in other half-metals also [16,27,59]. The small value of the gap could possibly be an indication of two-magnon scattering (2MS) [59] or anomalous magnon scattering (AMS) [18,19] which gives a power-law dependence or it could also be an indication of the gap signifying the magnon dispersion gap instead of spin-flip gap [16]. The location of the Fermi level is extremely sensitive to stoichiometry and crystal defects which may lead to variation in the gap. The time and spin resolved ultrafast

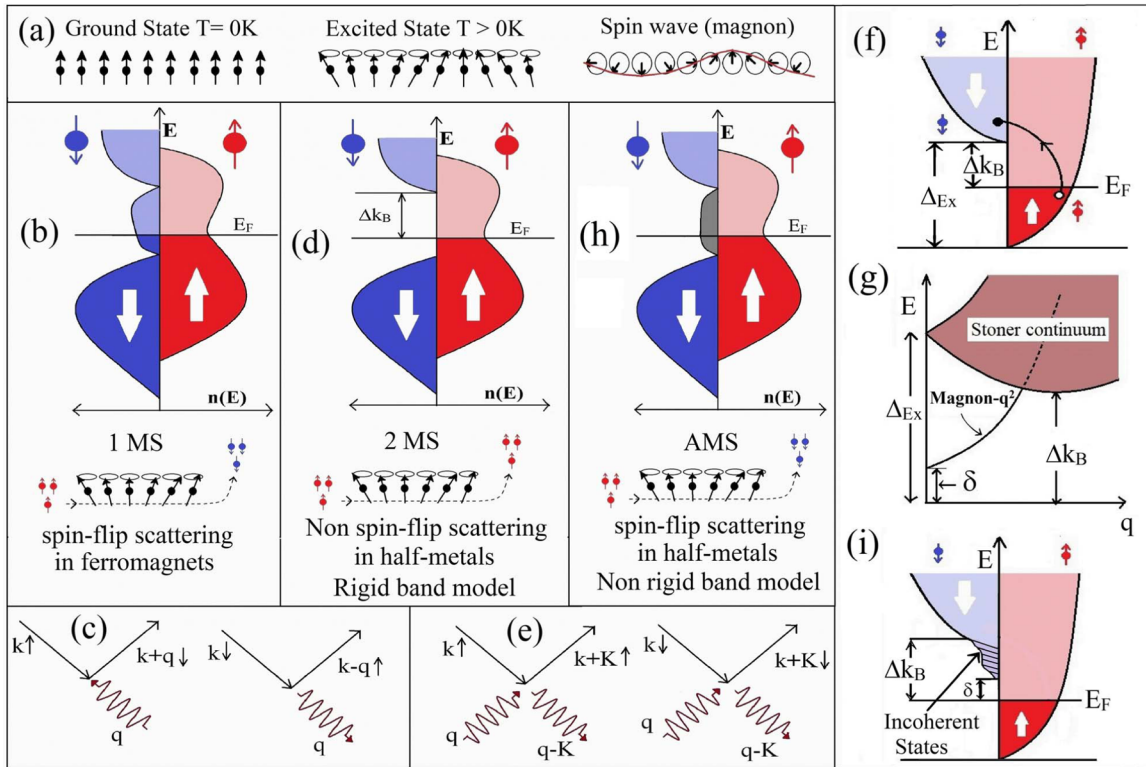


FIG. 3. (a) Schematic representation of the ground state of a ferromagnet with all spins aligned at 0 K; at finite temperatures spin waves are excited as shown in front and top view. (b) Schematic band diagram of itinerant ferromagnet, where red and blue color bands correspond to spin-up and spin-down electrons and the one-magnon spin-flip scattering is illustrated at the bottom. (c) Self-energy diagram [22] for spin-flip scattering/1MS. (d) Schematic band diagram of half-metal in rigid band model where 2MS takes place shown at the bottom. (e) Self-energy diagram of non-spin-flip scattering/2MS from electron-magnon interaction. (f) Exchange spin-split ( $\Delta_{Ex}$ ) bands with half-metallic gap ( $\Delta k_B$ ) at  $E_F$ ; arrow shows the Stoner spin-flip excitation of an electron. (g) Spin excitation spectrum of an anisotropic half-metallic itinerant ferromagnet;  $\Delta_{Ex}$  is spin-splitting energy at  $q = 0$  and  $\Delta k_B = \Delta_{Ex} - E_F$ . The black solid line shows the parabolic magnon dispersion ( $q^2$ ) for anisotropy gap ( $\delta$ ). (h) Band diagram of half-metal at finite temperature with temperature-induced (gray) spin minority band at  $E_F$  where AMS/spin-flip scattering is allowed as shown in the bottom. (i) Peculiar electronic structure of an anisotropic half-metal due to nonquasiparticle (incoherent) states [57,58] shown by a shaded portion that arises in the minority band gap above  $E_F$ . The absence of incoherent states in the energy range  $\delta$  above  $E_F$  is due to the anisotropy gap in magnon dispersion which freezes magnon excitation for  $k_B T < \delta$ .

spectroscopy experiments in  $\text{Co}_3\text{Sn}_2\text{S}_2$  show the presence of a spin-polarized gap of  $\approx 210$  meV above  $E_F$  due to annihilation of the Weyl node [60].

In a ferromagnetic system with localized moments, collective modes of spin excitation are termed as spin waves or magnons. In an itinerant ferromagnet, the spin excitations are collective like a ferromagnet with localized moments as well as single-particle Stoner spin-flip excitations [61,62]. A schematic representation of Stoner excitation and Stoner continuum for half-metallic ferromagnets is shown in Figs. 3(f) and 3(g), respectively. In half-metals, the spin-up and spin-down bands are separated by a large Hund's coupling ( $\Delta_{Ex}$ ) so the Stoner continuum lies at a higher energy state and the magnon spectrum or modes are well defined like localized moment ferromagnets [63–65]. In isotropic ferromagnets, collective excitations with arbitrarily small energy are possible and the magnon energy spectrum for the long-wavelength limit ( $q \rightarrow 0$ ) is given as  $E(q) = D_s q^2$ , where  $D_s$  is the spin stiffness constant [66,67]. This leads to  $\rho_M \propto T^2$ . In anisotropic ferromagnet, a minimum energy ( $\delta$ ) is required to turn the spins against the anisotropy field to excite the

magnons which modifies the magnon energy spectrum as  $E(q) = \delta + D_s q^2$ . The gap ( $\delta$ ) in the magnon spectrum suppresses the magnon population  $\langle n_q \rangle = [\exp(-E(q)/k_B T) - 1]^{-1}$  and electron-magnon scattering ( $\propto \sum n_q$ ) which modifies the electron-magnon resistivity as  $\rho_M \propto T^2 \exp(-\delta/k_B T)$  [37–40,68,69]. The exponential suppression of resistivity in Fig. 2(b) could also be due to suppression of electron-magnon scattering due to the anisotropic gap in the magnon spectrum. The gap  $\delta = 2.46(4)$  meV agrees well with the gap in the magnon spectrum of  $\text{Co}_3\text{Sn}_2\text{S}_2$  (2.3 meV) observed through neutron scattering experiments [47] at 4 K. The gap in the magnon spectrum arises due to spin anisotropy energy from spin-orbit coupling which is estimated as 0.6 meV for  $\text{Co}_3\text{Sn}_2\text{S}_2$ . The large gap in neutron scattering experiments suggests a significant contribution from modification [47–49] of spin-wave excitations by Weyl fermions [47]. The Weyl fermions modify the spin dynamics which affect the spin-wave dispersions, spin-wave gap, and spin-stiffness [47–49]. The gap in magnon dispersion in a magnetic Weyl semimetal at  $q = 0$  is given as  $\delta = Q/\alpha = Q/(\alpha_0 + \alpha_1)$ , where  $Q$  is due to spin anisotropy energy from spin-orbit coupling,  $\alpha$  is from

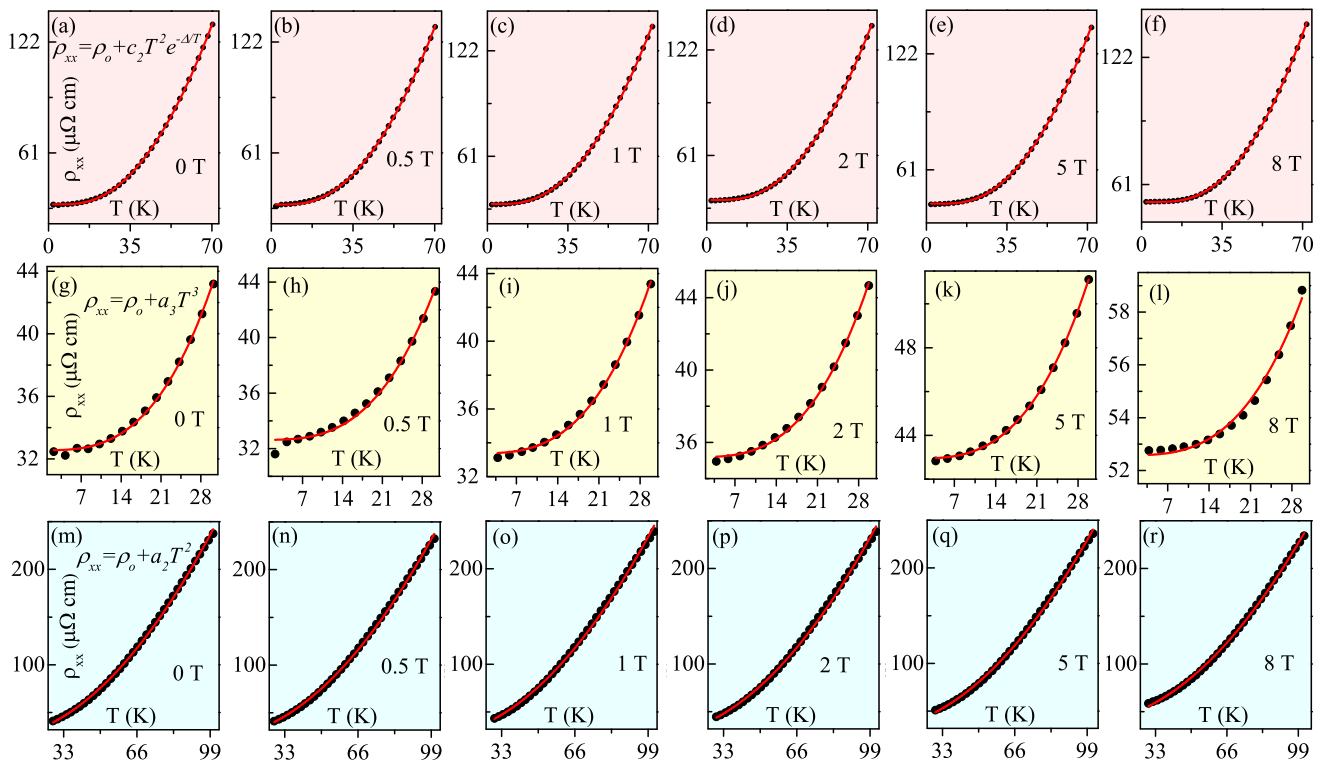


FIG. 4. (a)–(f) The temperature-dependent resistivity in range of 2–70 K at different constant magnetic fields. The red solid lines show the least-squares fitting of  $\rho_{xx} = \rho_0 + c_2 T^2 \exp(-\Delta/T)$  to data. (g)–(l) The resistivity versus temperature at different constant fields at  $T < \Delta$ . The solid lines show the fitting of  $\rho_{xx} = \rho_0 + a_3 T^3$ . (m)–(r) The temperature variation of resistivity for  $T > \Delta$  at different constant magnetic fields. The solid lines are the least-squares fitting of  $\rho_{xx} = \rho_0 + a_2 T^2$ .

the Berry phase term,  $\alpha_0$  is a finite contribution from bands without spin-orbit coupling, and  $\alpha_1 = \lambda \sigma_{xy}$  is the contribution from the shape ( $\lambda$ ) of Weyl cones and anomalous Hall conductivity ( $\sigma_{xy}$ ) from the Berry curvature of Weyl nodes [48,49].

Figure 2(c) shows the plot of  $\rho_{xx}$  versus  $T^2$  which is linear above the gap temperature ( $\Delta$ ) suggesting that  $T^2$  type spin-flip scattering is dominant in the higher temperature region. Below the gap temperature,  $\rho_{xx}$  deviates from  $T^2$  dependence indicating a change in scattering behavior. Similar crossovers are experimentally observed in other half-metals due to the deviation from one-magnon scattering [17,25,70–73]. For  $T \ll \Delta$ , Kubo [22] *et al.* proposed a two-magnon scattering (2MS) process for a perfect half-metal where the spin minority band is completely absent at  $E_F$  as shown in Fig. 3(d). The scattering of a spin-up conduction electron of momentum  $k$  by a spin-wave of initial momentum  $q$  gives a scattered spin-up state with momentum  $q + K$  leaving a spin-wave of final momentum  $q - K$  in the lattice. See Fig. 3(e). The resistivity from the two-magnon scattering process is  $\propto T^{9/2}$  at low temperatures which crosses over to  $T^{7/2}$  at high temperatures [20].  $\text{Co}_3\text{Sn}_2\text{S}_2$  does not follow the  $\rho_M \propto T^{9/2}$  or  $\rho_M \propto T^{7/2}$  scaling suggesting the two-magnon scattering process is not the dominant scattering mechanism and  $\text{Co}_3\text{Sn}_2\text{S}_2$  deviates from perfect polarization at low temperatures due to the presence of incoherent or minority states at  $E_F$  [19,57]. The small degree of spin polarization in  $\text{Co}_3\text{Sn}_2\text{S}_2$  is explained by the appearance of spin-down density of states at  $E_F$  when including spin-orbit coupling in calculations [8]. Deviation from 100% spin polarization can also occur from non-quasiparticle

(incoherent) states [20,57] shown in Fig. 3(i) which arise from spin-polaron processes. Due to the gap in magnon dispersion ( $\delta$ ) in an anisotropic half-metallic ferromagnet, magnon excitation requires finite thermal energy ( $k_B T > \delta$ ) and hence spin-up electron excitations are seized at low temperatures. In half-metallic ferromagnets, the superposition of spin-up electron excitation and virtual magnon enables the forbidden spin-down electron excitation which is known as the spin-polaron process. The incoherent states do not exist at  $E_F$  and depend on magnon frequencies. With the excitation of magnons ( $k_B T > \delta$ ), a tail of incoherent states will appear at a gap ( $\delta$ ) above  $E_F$  shown by the shaded portion in Fig. 3(i).

At finite temperature, Furukawa [18,19] proposed that local spin fluctuations in a half-metal create a thermally induced minority band at  $E_F$ . The electronic band structure of half-metal at  $T > 0$  K is modified as shown in Fig. 3(h) which allows the spin-flip scattering known as anomalous magnon scattering (AMS). The resistivity from AMS depends on magnon density ( $\delta m$ ) and density of states of minority spin band which also depend on  $\delta m$  [18,19,35,74], thus

$$\rho_M(T) \propto (\delta m)^2 \propto (T/D_s)^3, \quad (3)$$

where  $\delta m = [M(0) - M(T)]/M(0)$  and  $D_s$  is the spin stiffness coefficient.  $M(0)$  and  $M(T)$  are the saturated spin moments at 0 K and temperature  $T$ , respectively. Figure 2(d) shows the plot of  $\rho_{xx}$  versus  $T^3$  which fits well with  $\rho_{xx} = \rho_0 + a_3 T^3$  for  $T \leq \Delta$ . The  $T^3$  behavior of resistivity clearly shows the dominance of anomalous magnon scattering and the presence of the spin fluctuation induced minority band at  $E_F$

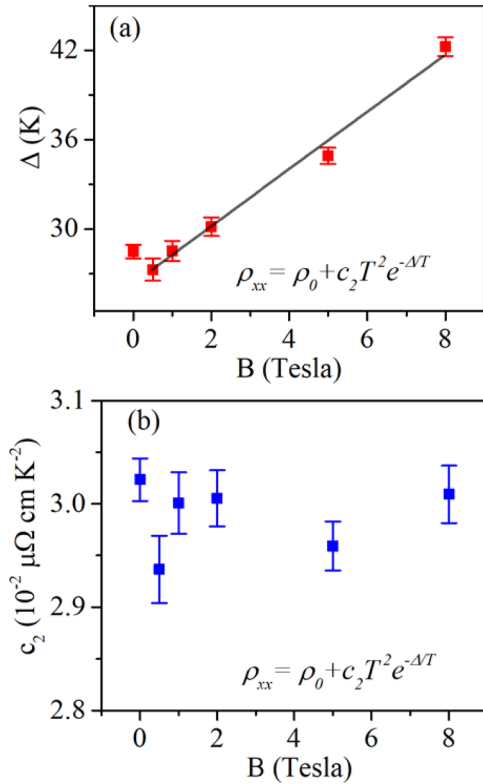


FIG. 5. (a) The magnetic field dependence of gap  $\Delta$  obtained from fitting of Figs. 4(a)–4(f). The black solid line is the linear fit of data above saturation field (0.5–8 T). (b) Change in magnon scattering strength  $c_2$  with the field.

in  $\text{Co}_3\text{Sn}_2\text{S}_2$ . The coefficient  $a_3 = 3.91 \times 10^{-4} \mu\Omega \text{ cm K}^{-3}$  is a measure of DOS of minority electrons at  $E_F$  or spin fluctuations in the system. From Eq. (3),  $a_3 \propto D_s^{-3}$ . AMS increases on decreasing the  $D_s$ , and on further lowering the  $D_s$ , 2MS becomes important [35]. Similar exponential suppression of one-magnon scattering  $T^2 \exp(-\Delta/T)$  along with low-temperature  $T^3$  behaviors are experimentally observed in other half-metals [16,24,75,76]. In comparison to Furukawa [19] who treated the Kubo formula inconsistently [57], Irkhin *et al.* [20] properly accounted the rotation symmetry requirements and arrived at  $T^{7/2}$  behavior which is consistent with Kubo's calculations [22]. Both theories have close exponents and experimentally, the  $T^3$  behavior is observed in several half-metals like  $\text{CrO}_2$  [16,24,28],  $\text{Fe}_2\text{TiSn}$  [75],  $\text{Fe}_2\text{CoSi}$  [76],  $\text{Co}_2\text{CrAl}$  [77,78],  $\text{Fe}_3\text{Si}$  [79–82],  $\text{Fe}_2\text{RhSi}$  [83],  $\text{Fe}_2\text{RhGe}$  [83],  $\text{Co}_{2-x}\text{Ru}_x\text{MnSi}$  [84,85],  $\text{Co-Mn-V-Al}$  [86],  $\text{CeAuSb}_2$  [71], and  $\text{R}_{0.6}\text{Sr}_{0.4}\text{MnO}_3$  [18,35] and largely considered as crucial evidence of half-metallic nature [19].

Figures 4(a)–4(f) show the temperature dependence of resistivity for  $T \leq 70$  K at different magnetic fields and the data are fitted with  $\rho_{xx} = \rho_0 + c_2 T^2 \exp(-\Delta/T)$ . The gap  $\Delta$  increases linearly with field as shown in Fig. 5(a). The half-metallic gap is due to large exchange splitting of spin subbands. The application of magnetic field increases the half-metallic gap by Zeeman-shifting the spin-up bands to lower energy and spin-down bands toward higher energy. For  $\text{Co}_3\text{Sn}_2\text{S}_2$ , the magnetic moment of  $\pm 1 \mu_B$  per spin-up/spin-down band suggests a Zeeman shifting of  $0.058 \text{ meV T}^{-1}$

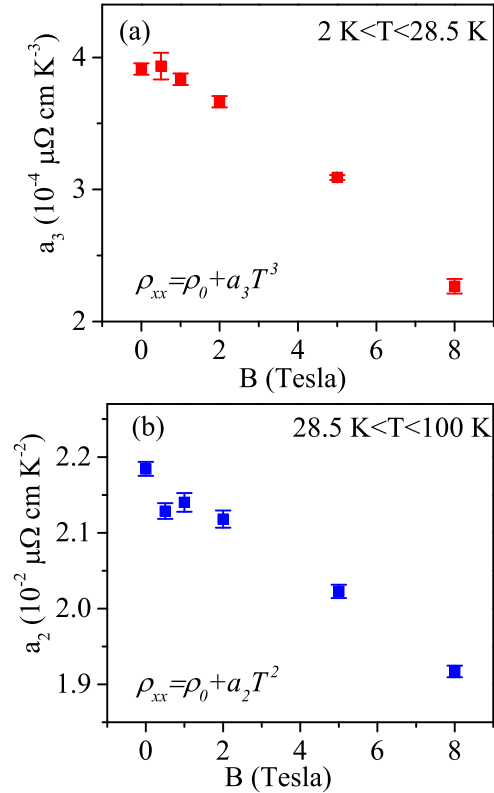


FIG. 6. (a) The magnetic field dependence of coefficient  $a_3$  (of  $T^3$ ) obtained from fitting of  $\rho_{xx} = \rho_0 + a_3 T^3$  to data of Figs. 4(m)–4(r). (b) The field variation of coefficient  $a_2$  (of  $T^2$ ) estimated from fitting of Figs. 4(g)–4(l).

to lower/higher energies [87]. The magnetic field greater than saturation field ( $\approx 0.05$  T) is applied along the crystal's easy  $c$  axis which does not alter the occupation of spin subbands [55,88]. From the linear fit of field dependence of  $\Delta$  we obtain field-induced spin splitting of  $\approx 0.166 \text{ meV T}^{-1}$ . Figure 5(b) shows that  $c_2$  is constant with field suggesting that field does not affect the strength of scattering process. The exponential suppression of temperature dependence of resistivity in Figs. 4(a)–4(f) at different magnetic fields can also be discussed in the form of electron-magnon scattering in anisotropic ferromagnets. The applied field enhances the gap in the magnon spectrum as  $E(q) = g\mu_B H + \delta + D_s q^2$  (for  $q \rightarrow 0$ ) where  $H$  is the internal magnetic field and  $g$  is the Landé  $g$  factor. Therefore, the field enhancement of the gap in Fig. 5(a) could also occur due to increase in the magnon spectrum gap in anisotropic ferromagnets and cannot help in further distinguishing the half-metallic or anisotropic ferromagnetic nature of the sample.

Figures 4(g)–4(l) exhibits the temperature variation of resistivity at different fields for  $T < \Delta$ . The resistivity fits well with  $\rho = \rho_0 + a_3 T^3$  and the field dependence of  $a_3$  is shown in Fig. 6(a). The magnetic field suppresses the spin fluctuations as well as the magnon density which reduces the strength of anomalous magnon scattering ( $a_3$ ). For  $T > \Delta$ , the resistivity at different fields fits well with  $\rho = \rho_0 + a_2 T^2$  as shown in Figs. 4(m)–4(r) and the field dependence of  $a_2$  is shown in Fig. 6(b). On increasing the magnetic field, the magnon exci-

tation energy increases which weakens the electron-magnon scattering.

#### IV. DISCUSSION

The temperature dependence of resistivity exhibits exponential suppression of spin-flip electron-magnon scattering. The suppression of electron-magnon scattering could occur for two possible cases, first a half-metal where magnons are present but spin minority band is absent, and second an anisotropic ferromagnet where magnon spectrum is gapped which quenches the magnon excitation at low temperatures. At  $T \geq 28.5$  K, normal ferromagnetic behavior is restored as evident by  $T^2$  behavior of electrical resistivity. For the case of half-metal, at  $T \leq 28.5$  K, anomalous magnon scattering (AMS) and double-magnon scattering (2MS) are the possible dominant scattering mechanisms and the  $T^3$  dependence of resistivity shows the dominance of anomalous magnon scattering. The anomalous magnon scattering suggests that  $\text{Co}_3\text{Sn}_2\text{S}_2$  is a half-metal, but has a thermally induced minority band at  $E_F$  in the temperature range of measurements. This is in agreement with the findings of Andreev reflection measurements where spin polarization of  $\sim 25\%$ – $50\%$  is observed at the Fermi level [8,14]. The soft itinerant magnetism in  $\text{Co}_3\text{Sn}_2\text{S}_2$  is predicted to show strong thermal spin fluctuations which decrease the magnetization below  $1 \mu_B$  per f.u. and diminish the half-metallicity [89]. The half-metallic gap is due to large exchange splitting of spin subbands and is typically in eV. Theoretically, a half-metallic gap of  $\approx 100$  meV is predicted [2] for  $\text{Co}_3\text{Sn}_2\text{S}_2$  while a significantly smaller gap of 2.46(4) meV is obtained from resistivity fitting. The field dependence of gap  $\approx 0.166 \text{ meV T}^{-1}$  is large in comparison to  $0.058 \text{ meV T}^{-1}$  expected [87] from Zeeman shift of spin-up/spin-down bands in  $\text{Co}_3\text{Sn}_2\text{S}_2$ . In a similar spin-orbit kagome magnet, large Zeeman splittings are attributed to a correlated magnetic topological phase [90]. The gap of 2.46(4) meV responsible for exponential suppression of electron-magnon scattering is close to the anisotropic gap of 2.3 meV observed in inelastic neutron scattering of  $\text{Co}_3\text{Sn}_2\text{S}_2$ . The temperature dependence of resistivity and the linear field dependence of the gap can be equally explained within the framework of anisotropic ferromagnet. The anisotropic gap

of 2.46(4) meV is large in comparison to the anisotropic gap of 0.6 meV estimated from spin-orbit coupling suggesting possible modification of spin dynamics from Weyl fermions. The suppression of electron-magnon scattering for a half-metal as well as anisotropic ferromagnet reduces the magnon contribution of resistivity at low temperatures making the contribution of electron-phonon, electron-defect, and Lorentz contributions more prominent. This causes a crossover from negative to positive magnetoresistance.

The appearance of incoherent states in a minority band gap allows the forbidden spin-flip scattering and causes deviation from 100% spin polarization. Furukawa [19] proposed the origin of electronic states in the minority band gap to thermally induced spin fluctuations which depend on magnon population, and later Irkhin *et al.* [57] suggested the origin of incoherent states in the minority band gap to the spin-polaron process which depends on magnon frequency [58]. The presence of a large anisotropic gap ( $\delta$ ) in magnon dispersion of half-metals at low temperatures ( $k_B T < \delta$ ) seizes the formation of magnons and suppresses the spin-flip electron-magnon scattering and can help in achieving the perfect spin polarization.

#### V. CONCLUSION

$\text{Co}_3\text{Sn}_2\text{S}_2$  is analyzed for electron-magnon scattering behaviors. The low-temperature magnon scattering behaviors are best described by an exponential suppression of spin-flip scattering. The resistivity behavior in  $\text{Co}_3\text{Sn}_2\text{S}_2$  can be separated into two regimes, first  $T > \Delta$  ( $\Delta = 28.5$  K) where spin-flip or one-magnon scattering is dominant and second  $T < \Delta$  where anomalous magnon scattering is dominant. The in-field analysis supports the half-metallic behavior. These are compelling pieces of evidence for  $\text{Co}_3\text{Sn}_2\text{S}_2$  to be referred to as a half-metal. Interestingly,  $\text{Co}_3\text{Sn}_2\text{S}_2$  is an anisotropic ferromagnet with a large anisotropic gap mediated by Weyl fermions which can give similar resistivity and in-field behaviors.

#### ACKNOWLEDGMENTS

D.K. acknowledges research grant from SERB India for Early Career Research Award (Grant No. ECR/2017/003350).

- 
- [1] R. Wehrich and I. Anusca, *Z. Anorg. Allg. Chem.* **632**, 1531 (2006).
- [2] E. Liu, Y. Sun, N. Kumar, L. Muechler, A. Sun, L. Jiao, S. Y. Yang, D. Liu, A. Liang, Q. Xu, J. Kroder, V. Süß, H. Borrmann, C. Shekhar, Z. Wang, C. Xi, W. Wang, W. Schnelle, S. Wirth, Y. Chen *et al.*, *Nat. Phys.* **14**, 1125 (2018).
- [3] Q. Xu, E. Liu, W. Shi, L. Muechler, J. Gayles, C. Felser, and Y. Sun, *Phys. Rev. B* **97**, 235416 (2018).
- [4] D. F. Liu, A. J. Liang, E. K. Liu, Q. N. Xu, Y. W. Li, C. Chen, D. Pei, W. J. Shi, S. K. Mo, P. Dudin, T. Kim, C. Cacho, G. Li, Y. Sun, L. X. Yang, Z. K. Liu, S. S. P. Parkin, C. Felser, and Y. L. Chen, *Science* **365**, 1282 (2019).
- [5] N. Morali, R. Batabyal, P. K. Nag, E. Liu, Q. Xu, Y. Sun, B. Yan, C. Felser, N. Avraham, and H. Beidenkopf, *Science* **365**, 1286 (2019).
- [6] Q. Wang, Y. Xu, R. Lou, Z. Liu, M. Li, Y. Huang, D. Shen, H. Weng, S. Wang, and H. Lei, *Nat. Commun.* **9**, 3681 (2018).
- [7] E. H. da Silva Neto, *Science* **365**, 1248 (2019).
- [8] S. Howlader, S. Saha, R. Kumar, V. Nagpal, S. Patnaik, T. Das, and G. Sheet, *Phys. Rev. B* **102**, 104434 (2020).
- [9] R. Wehrich, W. Yan, J. Rothballer, P. Peter, S. M. Rommel, S. Haumann, F. Winter, C. Schwickert, and R. Pöttgen, *Dalton Trans.* **44**, 15855 (2015).
- [10] J. M. D. Coey and S. Sanvito, *J. Phys. D: Appl. Phys.* **37**, 988 (2004).

- [11] M. Holder, Y. S. Dedkov, A. Kade, H. Rosner, W. Schnelle, A. Leithe-Jasper, R. Weihrich, and S. L. Molodtsov, *Phys. Rev. B* **79**, 205116 (2009).
- [12] Y. S. Dedkov, M. Holder, S. L. Molodtsov, and H. Rosner, *J. Phys.: Conf. Ser.* **100**, 072011 (2008).
- [13] L. Jiao, Q. Xu, Y. Cheon, Y. Sun, C. Felser, E. Liu, and S. Wirth, *Phys. Rev. B* **99**, 245158 (2019).
- [14] H. Wang, Y. Z. Liu, H. B. Zhou, H. R. Ji, J. W. Luo, J. W. Zhang, T. H. Wei, P. Y. Wang, S. Jia, and J. Wang, *Sci. China Phys. Mech. Astron.* **63**, 287411 (2020).
- [15] J. M. D. Coey and C. L. Chien, *MRS Bull.* **28**, 720 (2003).
- [16] J. M. D. Coey and M. Venkatesan, *J. Appl. Phys.* **91**, 8345 (2002).
- [17] A. Barry and J. M. D. Coey, *J. Appl. Phys.* **83**, 7166 (1998).
- [18] N. Furukawa, Y. Shimomura, T. Akimoto, and Y. Moritomo, *J. Magn. Magn. Mater.* **226-230**, 782 (2001).
- [19] N. Furukawa, *J. Phys. Soc. Jpn.* **69**, 1954 (2000).
- [20] V. Y. Irkhin and M. I. Katsnelson, *Eur. Phys. J. B* **30**, 481 (2002).
- [21] V. Y. Irkhin and M. I. Katsnelson, *Phys. Usp.* **37**, 659 (1994).
- [22] K. Kubo and N. Ohata, *J. Phys. Soc. Jpn.* **33**, 21 (1972).
- [23] D. Bombor, C. G. F. Blum, O. Volkonskiy, S. Rodan, S. Wurmehl, C. Hess, and B. Büchner, *Phys. Rev. Lett.* **110**, 066601 (2013).
- [24] A. Gupta, X. W. Li, and G. Xiao, *J. Appl. Phys.* **87**, 6073 (2000).
- [25] M. S. Anwar and J. Aarts, *Phys. Rev. B* **88**, 085123 (2013).
- [26] K. Suzuki and P. M. Tedrow, *Phys. Rev. B* **58**, 11597 (1998).
- [27] S. M. Watts, S. Wirth, S. von Molnár, A. Barry, and J. M. D. Coey, *Phys. Rev. B* **61**, 9621 (2000).
- [28] L. Xie, J. Z. Zhang, N. Y. Cui, and H. G. Zhang, *Surf. Rev. Lett.* **21**, 1450055 (2014).
- [29] J. C. Prestigiacomo, D. P. Young, P. W. Adams, and S. Stadler, *J. Appl. Phys.* **115**, 043712 (2014).
- [30] R. P. Dulal, B. R. Dahal, A. Forbes, N. Bhattarai, I. L. Pegg, and J. Philip, *Sci. Rep.* **9**, 3342 (2019).
- [31] Y. Venkateswara, D. Rani, K. G. Suresh, and A. Alam, *J. Magn. Magn. Mater.* **502**, 166536 (2020).
- [32] P. Nehla, C. Ulrich, and R. S. Dhaka, *J. Alloys Compd.* **776**, 379 (2019).
- [33] K. Srinivas, T. P. Kumari, M. M. Raja, and S. V. Kamat, *J. Appl. Phys.* **114**, 033911 (2013).
- [34] M. Jaime, P. Lin, M. B. Salamon, and P. D. Han, *Phys. Rev. B* **58**, R5901 (1998).
- [35] T. Akimoto, Y. Moritomo, A. Nakamura, and N. Furukawa, *Phys. Rev. Lett.* **85**, 3914 (2000).
- [36] X. Wang and X. G. Zhang, *Phys. Rev. Lett.* **82**, 4276 (1999).
- [37] M. B. Fontes, J. C. Trochez, B. Giordanengo, S. L. Bud'ko, D. R. Sanchez, E. M. Baggio-Saitovitch, and M. A. Continentino, *Phys. Rev. B* **60**, 6781 (1999).
- [38] A. R. Mackintosh, *Phys. Lett.* **4**, 140 (1963).
- [39] N. H. Sze, K. V. Rao, and G. T. Meaden, *J. Low Temp. Phys.* **1**, 563 (1969).
- [40] R. P. Jena and A. Lakhani, *J. Phys.: Conf. Ser.* **755**, 012030 (2016).
- [41] N. H. Andersen and H. Smith, *J. Phys., Colloq.* **39**, C6 (1978).
- [42] N. Hessel-Andersen and H. Smith, *Phys. Rev. B* **19**, 384 (1979).
- [43] J. Larrea J., M. B. Fontes, A. D. Alvarenga, E. M. Baggio-Saitovitch, T. Burghardt, A. Eichler, and M. A. Continentino, *Phys. Rev. B* **72**, 035129 (2005).
- [44] D. Schulze-Grachtrup, M. Bleckmann, B. Willenberg, S. Süllow, M. Bartkowiak, Y. Skourski, H. Rakoto, I. Sheikin, and J. A. Mydosh, *Phys. Rev. B* **85**, 054410 (2012).
- [45] A. Maurya, R. Kulkarni, S. K. Dhar, and A. Thamizhavel, *J. Phys.: Condens. Matter* **25**, 435603 (2013).
- [46] A. Maurya, P. Bonville, A. Thamizhavel, and S. K. Dhar, *J. Phys.: Condens. Matter* **27**, 366001 (2015).
- [47] C. Liu, J. Shen, J. Gao, C. Yi, D. Liu, T. Xie, L. Yang, S. Danilkin, G. Deng, W. Wang, S. Li, Y. Shi, H. Weng, E. Liu, and H. Luo, *Sci. China Phys. Mech. Astron.* **64**, 217062 (2021).
- [48] S. Itoh, Y. Endoh, T. Yokoo, S. Ibuka, J. G. Park, Y. Kaneko, K. S. Takahashi, Y. Tokura, and N. Nagaosa, *Nat. Commun.* **7**, 11788 (2016).
- [49] K. Jenni, S. Kunkemöller, D. Brüning, T. Lorenz, Y. Sidis, A. Schneidewind, A. A. Nugroho, A. Rosch, D. I. Khomskii, and M. Braden, *Phys. Rev. Lett.* **123**, 017202 (2019).
- [50] S. Rathod, Megha, A. Lakhani, and D. Kumar, *AIP Conf. Proc.* **2220**, 060007 (2020).
- [51] S. Rathod, Megha, A. Lakhani, and D. Kumar, *J. Solid State Chem.* **289**, 121461 (2020).
- [52] A. Bid, A. Bora, and A. K. Raychaudhuri, *Phys. Rev. B* **74**, 035426 (2006).
- [53] W. Schnelle, A. Leithe-Jasper, H. Rosner, F. M. Schappacher, R. Pöttgen, F. Pielhofer, and R. Weihrich, *Phys. Rev. B* **88**, 144404 (2013).
- [54] T. Izuyama, D. J. Kim, and R. Kubo, *J. Phys. Soc. Jpn.* **18**, 1025 (1963).
- [55] K. Zakeri, *Phys. Rep.* **545**, 47 (2014).
- [56] T. Kasuya, *Prog. Theor. Phys.* **22**, 227 (1959).
- [57] V. Y. Irkhin, M. I. Katsnelson, and A. I. Lichtenstein, *J. Phys.: Condens. Matter* **19**, 315201 (2007).
- [58] M. I. Katsnelson, V. Y. Irkhin, L. Chioncel, A. I. Lichtenstein, and R. A. de Groot, *Rev. Mod. Phys.* **80**, 315 (2008).
- [59] V. V. Marchenkov and V. Y. Irkhin, *Phys. Met. Metallogr.* **122**, 1133 (2021).
- [60] F. Sun, T. Zhang, C. J. Yi, Y. L. Wu, H. Zhao, Q. Wu, Y. G. Shi, H. Weng, and J. Zhao, *Phys. Rev. B* **104**, L100301 (2021).
- [61] Y. Ishikawa, G. Shirane, J. A. Tarvin, and M. Kohgi, *Phys. Rev. B* **16**, 4956 (1977).
- [62] P. Dai, H. Y. Hwang, J. Zhang, J. A. Fernandez-Baca, S.-W. Cheong, C. Kloc, Y. Tomioka, and Y. Tokura, *Phys. Rev. B* **61**, 9553 (2000).
- [63] N. Furukawa, *J. Phys. Soc. Jpn.* **65**, 1174 (1996).
- [64] L. Vasiliu-Doloc, J. W. Lynn, A. H. Moudden, A. M. de Leon Guevara, and A. Revcolevschi, *Phys. Rev. B* **58**, 14913 (1998).
- [65] V. Y. Irkhin and M. I. Katsnelson, *J. Phys.: Condens. Matter* **2**, 7151 (1990).
- [66] F. G. Eich, S. Pittalis, and G. Vignale, *Eur. Phys. J. B* **91**, 173 (2018).
- [67] F. Keffer, H. Kaplan, and Y. Yafet, *Am. J. Phys.* **21**, 250 (1953).
- [68] L. Benito, R. C. C. Ward, and M. G. Blamire, *Phys. Rev. B* **88**, 224407 (2013).
- [69] R. P. Jena and A. Lakhani, *J. Magn. Magn. Mater.* **448**, 367 (2018).
- [70] V. V. Marchenkov, Y. A. Perevozchikova, N. I. Kourov, V. Y. Irkhin, M. Eisterer, and T. Gao, *J. Magn. Magn. Mater.* **459**, 211 (2018).
- [71] L. Balicas, S. Nakatsuji, H. Lee, P. Schlottmann, T. P. Murphy, and Z. Fisk, *Phys. Rev. B* **72**, 064422 (2005).
- [72] S. J. Liu, S. F. Chen, J. Y. Juang, J. Y. Lin, K. H. Wu, T. M. Uen, and Y. S. Gou, *Jpn. J. Appl. Phys.* **46**, 6621 (2007).

- [73] M. B. Salamon and M. Jaime, *Rev. Mod. Phys.* **73**, 583 (2001).
- [74] R. Skomski and P. A. Dowben, *Eur. Phys. Lett.* **58**, 544 (2002).
- [75] S. Chaudhuri, D. Salas, V. Srihari, E. Welter, I. Karaman, and P. A. Bhobe, *Sci. Rep.* **11**, 524 (2021).
- [76] Y. Du, G. Z. Xu, X. M. Zhang, Z. Y. Liu, S. Y. Yu, E. K. Liu, W. H. Wang, and G. H. Wu, *Europhys. Lett.* **103**, 37011 (2013).
- [77] M. Zhang, Z. Liu, H. Hu, G. Liu, Y. Cui, J. Chen, G. Wu, X. Zhang, and G. Xiao, *J. Magn. Magn. Mater.* **277**, 130 (2004).
- [78] A. Datta, M. Modak, M. M. Patidar, V. Ganesan, and S. Banerjee, *AIP Conf. Proc.* **2265**, 030455 (2020).
- [79] J. Thomas, J. Schumann, H. Vinzelberg, E. Arushanov, R. Engelhard, O. G. Schmidt, and T. Gemming, *Nanotechnology* **20**, 235604 (2009).
- [80] H. Vinzelberg, J. Schumann, D. Elefant, E. Arushanov, and O. G. Schmidt, *J. Appl. Phys.* **104**, 093707 (2008).
- [81] J. Xie, Y. Liao, D. Wu, and Q. Xie, *Vacuum* **191**, 110325 (2021).
- [82] J. Xie, Y. Liao, D. Wu, and Q. Xie, *J. Magn. Magn. Mater.* **530**, 167904 (2021).
- [83] Y. Venkateswara, S. S. Samatham, A. K. Patel, P. D. Babu, M. R. Varma, K. G. Suresh, and A. Alam, *Phys. Rev. B* **104**, 094402 (2021).
- [84] H. P. Zhang, W. B. Liu, X. F. Dai, X. M. Zhang, H. Y. Liu, X. Yu, and G. D. Liu, *IUCrJ* **7**, 113 (2020).
- [85] H. Pandey and R. C. Budhani, *J. Appl. Phys.* **113**, 203918 (2013).
- [86] L. Y. Wang, X. F. Dai, X. T. Wang, Y. T. Cui, E. K. Liu, W. H. Wang, G. H. Wu, and G. D. Liu, *Mater. Res. Express* **2**, 106101 (2015).
- [87] J. X. Yin, N. Shumiya, Y. Jiang, H. Zhou, G. Macam, H. O. M. Sura, S. S. Zhang, Z. J. Cheng, Z. Guguchia, Y. Li, Q. Wang, M. Litskevich, I. Belopolski, X. P. Yang, T. A. Cochran, G. Chang, Q. Zhang, Z. Q. Huang, F. C. Chuang, H. Lin *et al.*, *Nat. Commun.* **11**, 4415 (2020).
- [88] L. Ranno, A. Barry, and J. M. D. Coey, *J. Appl. Phys.* **81**, 5774 (1997).
- [89] I. V. Solovyev, S. A. Nikolaev, A. V. Ushakov, V. Yu. Irkhin, A. Tanaka, and S. V. Streltsov, *Phys. Rev. B* **105**, 014415 (2022).
- [90] J. X. Yin, S. S. Zhang, H. Li, K. Jiang, G. Chang, B. Zhang, B. Lian, C. Xiang, I. Belopolski, H. Zheng, T. A. Cochran, S. Y. Xu, G. Bian, K. Liu, T. R. Chang, H. Lin, Z. Y. Lu, Z. Wang, S. Jia, W. Wang *et al.*, *Nature (London)* **562**, 91 (2018).